Prabha Materials Science Letters
Vol. 4, No. 1, 4-13, 2025
https://doi.org/10.33889/PMSL.2025.4.1.002

Ram Arti Publishers

Synthesis of Molybdenum Disulfide-Polyvinyl Alcohol Nanocomposite and Detailed Study of Its Optical Properties

A. Dhariwal
Thin Film and Nanotechnology Laboratory,
Department of Physics, Faculty of Engineering and Computing Sciences,
Teerthanker Mahaveer University, Moradabad, 244001, Uttar Pradesh, India.
E-mail: anjali16rajput1998@gmail.com

D. Banerjee
Thin Film and Nanotechnology Laboratory,
Department of Physics, Faculty of Engineering and Computing Sciences,
Teerthanker Mahaveer University, Moradabad, 244001, Uttar Pradesh, India.
Corresponding author: nilju82@gmail.com

(Received on September 29, 2024; Revised October 19, 2024 & October 24, 2024; Accepted on October 28, 2024)

Abstract
The present study investigates the optical and electronic properties of molybdenum disulfide-polyvinyl alcohol (MoS_2-PVA) nanocomposites. Cauliflower-like fractal MoS_2 nanostructures were synthesized through a hydrothermal method using sodium molybdate and L-cystine as precursors. These synthesized nanostructures were then incorporated into PVA polymer chains to develop PVA-MoS_2 composites. The X-ray diffraction analysis confirmed the successful phase formation of the nanocomposites, while field emission scanning electron microscopic images revealed the one-dimensional structure of the system. UV-Vis transmittance spectra were utilized to determine the band gap of the materials through Tauc plots. Fourier transform infrared spectroscopy indicated the presence of specific chemical bonds and demonstrated significant changes in the vibrational energy levels of the pure polymer upon composite formation. Energy-dispersive X-ray (EDX) analysis with elemental mapping shows that the material maintained required stoichiometry. Thermogravimetric analysis of pure MoS_2 demonstrates excellent thermal stability, withstanding temperatures as high as 700° C. This comprehensive study adds valuable insights to the existing literature on nanocomposite materials.

Keywords- MoS_2, PVA, Nanocomposites, Optical, Electronic.

1. Introduction

Graphene, the first discovered two-dimensional (2D) material, exhibits remarkable electrical properties and a unique chemical structure. This breakthrough led to the discovery of other similar materials, such as transition metal dichalcogenides (TMDs) (Mas-Balleste et al., 2011). These 2D materials have demonstrated promising electronic properties, making them suitable for applications in devices such as thin-film transistors (TFTs), OLEDs, optoelectronics, and sensors (Chang and Wu, 2013; Das et al., 2014; Hwang et al., 2012; Pawbake et al., 2016). In recent years, quasi-2D materials like WSe_2, WS_2, MoS_2, and $MoSe_2$ have attracted significant research interest due to their immense potential in nanotechnology and nanoscience for various applications. Structurally, these materials consist of two-dimensional layers of sandwiched sheets, where atoms are covalently bonded within each layer, while weak Van der Waals forces hold the stacked layers together (Cheng et al., 2016).

Among these 2D materials, MoS_2 stands out as a highly promising candidate for electronic device applications due to its advantageous quantum confinement and high charge mobility. This is largely due to its direct band gap of 1.85 eV in monolayers and an indirect band gap of 1.29 eV in multilayers (Shinde et al., 2014). MoS_2 can exist in different phases, such as 1T (metallic phase), 2H (hexagonal symmetry), and

3R (rhombohedral), depending on the stacking of single, double, and triple layers. The hexagonal structure of molybdenum atoms sandwiched between sulphur atoms is consistent across these phases. With rapid advancements in the development of 2D materials for future devices, various synthesis methods for monolayer and few-layer MoS_2 flakes have emerged, including micromechanical exfoliation, hydrothermal processing, solution-based chemical exfoliation, chemical vapor deposition, ion intercalation exfoliation, and sulfurization of molybdenum (Gu et al., 2016; Mak et al., 2010; Radisavljevic et al., 2011; Wang et al., 2013; Zhou et al., 2011). Exfoliated MoS_2 exhibits outstanding electrical properties and mechanical strength, making it ideal for microelectronic devices such as lasers, supercapacitors, TFTs, phototransistors, biosensors, solar cells, and batteries (Acerce et al., 2015; Huang et al., 2015; Kim et al., 2015; Tsai et al., 2014; Wei et al., 2016; Xiao et al., 2011; Yin et al., 2012).

Polyvinyl alcohol (PVA) is a semi-crystalline, water-soluble material with low electrical conductivity and is widely used in technological, pharmaceutical, and biomedical applications. Researchers have reported enhancements in the optical, thermal, dielectric, and electrical properties of MoS_2-based PVA nanocomposites synthesized through various methods. Anand et al. (2023) synthesized MoS_2/PVA nanocomposites with different concentrations of MoS_2 nanoparticles embedded in the polymer matrix to study their linear and non-linear optical properties (Anand et al., 2023). Similarly, A. Ratan et al. fabricated an asymmetric supercapacitor using a MoS_2-PVA nanocomposite film and a flexible graphite sheet as electrode materials (Ratan et al., 2021).

However, despite these advances, there is limited exploration of the impact of MoS_2 concentration on the tunability of optical properties in MoS_2-PVA nanocomposites, especially using a simple and scalable solution casting method. This study addresses this gap by focusing on the synthesis and comprehensive characterization of PVA-MoS_2 nanocomposite films, offering a low-cost, efficient approach to tune the optical properties of PVA-based materials. The prominent new outcomes that this study results are firstly, polymer like PVA welcomes the inclusion of MoS_2 by offering a significant interaction as a result of which there is significant shifts of various vibrational energy level; secondly by changing the MoS_2 content in polymer matrix the optical band gap may be tuned thereby manipulation of the entire opto-electronic properties of the composites is possible. Further, though directly not studied here, this study opens up possibilities to monitor the morphology, crystallinity, thermal stability as well as surface profile of the polymer by reinforcement with foreign material.

In this work MoS_2 nanoparticles were synthesized using a hydrothermal method. The PVA films and PVA-MoS_2 composite films were prepared using a simple, low-cost solution casting method. The samples were characterized using XRD, FESEM, FTIR, SEM with EDX, UV-Vis spectroscopy, and TG-DTA.

2. Experimental Methods

2.1 Substrate Cleaning

The glass substrates were initially cleaned with soap and dilute HCl. Then after the glass substrates were immersed in a 3:1 mixture of H_2SO_4 and HNO_3, covered, and heated until bubbling commenced. The substrates were kept under the same condition for three hours, then allowed to cool before being thoroughly rinsed with deionised (DI) water and dried. Silicon substrates were treated by immersing them in HF to remove the oxide layer, followed by placing it into ethanol and ultrasonication for 30 minutes. Rinsed it off with DI water and dried using tissue paper.

2.2 Synthesis of Molybdenum Disulfide

MoS_2 was synthesized using an in-situ hydrothermal method. For the preparation, an amount of sodium molybdate and L-cysteine maintaining 1:2 ratio was dissolved in 125 ml of DI water with continuous

stirring. The resulting suspension was transferred to a Teflon-lines stainless-steel autoclave and subjected to hydrothermal treatment at 200° C for 24 hours. After cooling naturally to room temperature, the product was filtered and rinsed with DI water. The final material was obtained by drying the residue at 60° C for 5 hours.

2.3 Synthesis of MoS_2-PVA Nanocomposite

A pure PVA thin film was prepared by dissolving 0.5 g of PVA in 80 ml of DI water and stirring the solution overnight at 60° C. The solution was then poured into petri dish containing pre-cleaned silicon and glass substrates. The setup was left undisturbed overnight to allow the solution to form a gel, and as the water evaporated, the gel adhered to the substrate as a thick film.

For the preparation of MoS_2-PVA sample, the same procedure was followed, except 0.1 mg of the previously synthesized MoS_2 was incorporated into the PVA solution before deposition.

Pure PVA and MoS_2-PVA composite was named as sample S1 and S2 respectively.

3. Results and Discussions

3.1 XRD Analysis

Figure 1 presents the XRD patterns for both samples S1 and S2, obtained through a standard θ-2θ scan within the range of 10° to 60°. In both cases, the absence of sharp peaks indicates the semi-crystalline nature of the samples, which is typical for PVA (Banerjee et al., 2012). Sample S1 exhibits a weak XRD signal centred on 19.9°, corresponds to the (101) plane of pure PVA. In sample S2, the reduced FWHM of the same peak suggests slight enhancement in the crystallinity and thus further predicts an interaction between MoS_2 and the PVA matrix. Similar crystallinity enhancement in polymer after reinforcement with proper guest material is not new and reported by other researchers (Banerjee et al., 2012; Chen et al., 2005; Naebe et al., 2008). According to the explanation came from other group here MoS_2 acts as nucleation sites which help polymers to enhance its crystallinity. The feeble peak observed at 14.28°, corresponding to the (002) plane of MoS_2, indicates the formation of hexagonal MoS_2 crystal but with very less periodicity, likely due to the synthesis conditions.

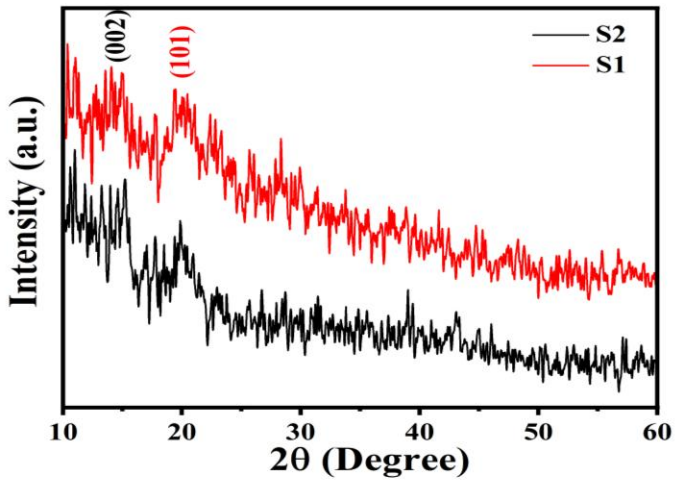

Figure 1. XRD patterns of samples S1 and S2.

3.2 Morphological Studies

Figure 2 (a, b) shows FESEM images of pure MoS_2 at different magnifications. The images reveal a uniform, cluster-like structure across the entire field of view, confirming the uniformity of the synthesized material. At higher magnification, these clusters are observed to resemble a cauliflower-like morphology.

Figure 2 (c, d) and **Figure 2 (e, f)** display the FESEM images of pure PVA and MoS_2-PVA thin films, respectively, deposited on silicon substrates. Both samples exhibit featureless, cluster-like morphologies, which is typical for polymeric materials. The FESEM images of pure PVA reveal a relatively smooth, featureless morphology with a cluster-like appearance. This type of morphology is common in polymeric materials, where the absence of significant surface features suggests a uniform distribution of polymer matrix. The cluster seen in the images indicate typical polymer agglomeration during film formation.

Whereas, in the composite, it is suggested that the presence of MoS_2 may influence the overall morphology, potentially altering the polymer structure. MoS_2 particles may appear as small, scattered regions within the PVA matrix, potentially forming a more defined, layered structure or contributing to enhanced roughness. The interaction between PVA and MoS_2 likely contributes to changes in surface texture, indicating improved material integration and composite formation.

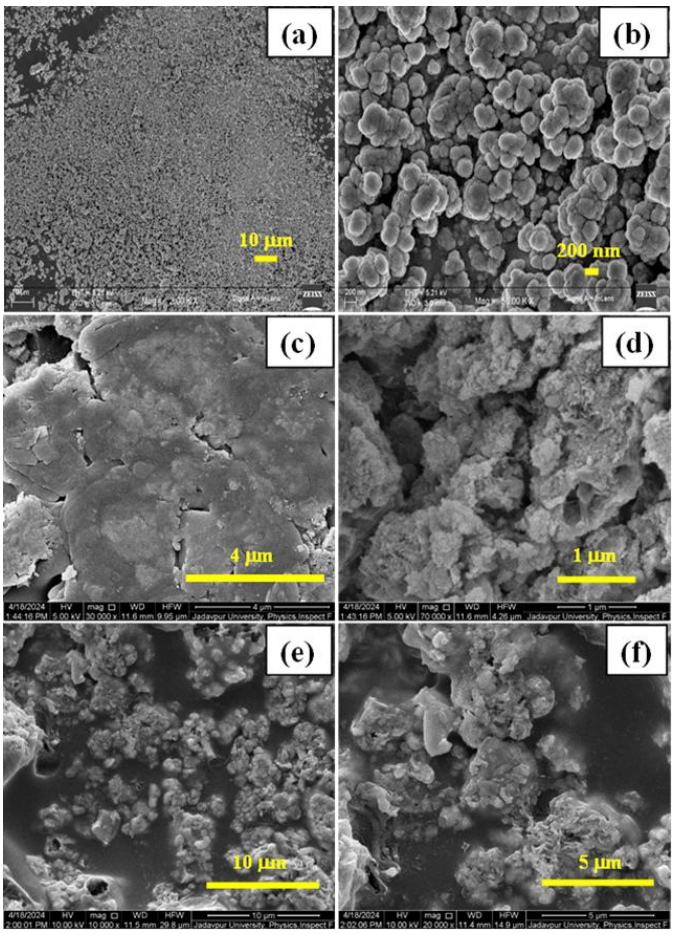

Figure 2. FESEM images of pure MoS_2 (a, b); pure PVA; (c, d) and MoS_2-PVA nanocomposite (e, f).

3.3 EDX Study

Energy-dispersive X-ray spectroscopy (EDX) analysis was performed to determine the stoichiometric ratio of the composite, with the corresponding spectrum and elemental mapping shown in **Figure 3 (a)** and **Figure 3 (b)**. The elemental composition of the sample, as obtained from the EDX analysis, is summarized in **Table 1**. The results indicate that the sample is of high purity, as only peaks corresponding to the desired elements were detected.

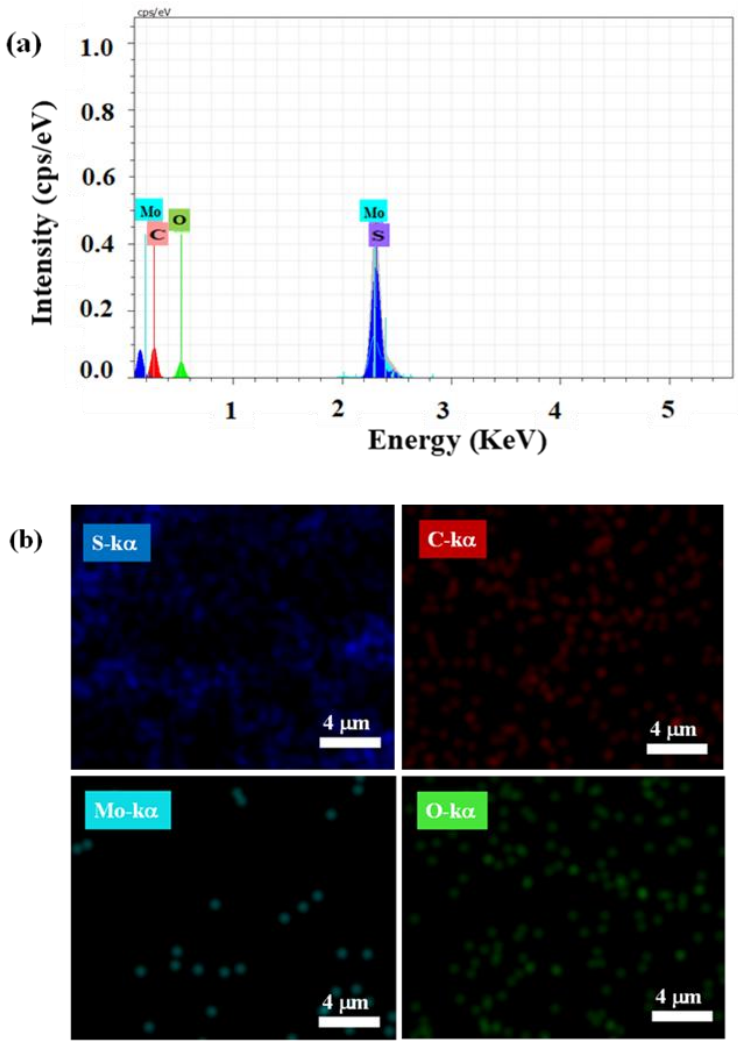

Figure 3. EDX spectrum (a) and Elemental mapping (b) of MoS_2-PVA nanocomposite.

Table 1. Compositional analysis of MoS_2-PVA nanocomposite.

Sample	Element	Atomic (%)	Weight (%)	Atomic Ratio
S2	**Mo**	7.27	29.36	Mo/S = 0.49
	S	14.76	23.23	
	C	44.00	21.88	
	O	29.97	25.53	

3.4 FTIR Study

Figure 4 presents the FTIR spectra of both the samples S1 and S2, recorded in absorbance mode within the wavenumber range of 400-3700 cm^{-1}, with a resolution of 4 cm^{-1}. Both samples exhibit similar patterns with a broad band in the higher wavenumber region (> 3000 cm^{-1}) which is attributed to the O-H bond. The peak at 2900 cm^{-1} present in the spectra of both the samples corresponds to C-H_n. The FTIR signal between 830-860 cm^{-1} is the signature of C-H/C=C bending vibrational energy level.

However, it should be noted that though these peaks are present in both the sample but variation in terms of intensity as well as position (Peak shift) can clearly be seen for sample S1 and S2. For instance, the C-H_n signal is considerably strong in case of sample S2 or the peak at lower wavenumber region shows a clearly shifting towards higher wavenumber region for the sample S2. Most importantly the strongest peak for the pure PVA that comes around 1277 cm^{-1} and carries the signature of C=C/C-H bond got completely disappeared in case of sample S2 (Ray et al., 2024). All these collectively suggest active interaction between the polymer and reinforcement material supporting the XRD results.

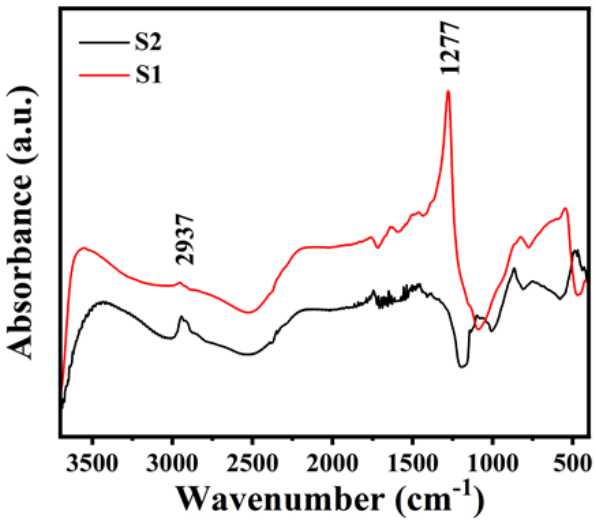

Figure 4. FTIR plot of samples S1 and S2.

3.5 UV-Vis Analysis and Tauc's Plot

Figure 5 (a) displays the UV-Vis spectra of both the samples, measured in transmittance mode across the entire range from the Visible to UV regions. Both samples exhibit similar spectral profiles, with transmittance around 50% for sample S1, which gradually decreases from visible to UV region, showing a significant drop near 400nm. Sample S2 presents a similar spectral pattern, but with a notably reduced transmittance. This is expected, as the incorporation of MoS_2 into the polymer matrix reduces light transmission. The optical band gap of both samples was determined using Tauc plot, shown in **Figure 5 (b)**. The data reveal that the optical band gap of pure PVA decreases from 3.44 eV to 3.18 eV after the addition of MoS_2 in sample S2. The changes in the band gap suggests that there must be change in the cluster sizes of sample and the reduction of the band gap shows the cluster size in case of sample S2 is greater which is rather expected when the polymer matrix has a significant interaction with the foreign compound. Thus, the reduction of band gap may in principle be attributed to the reverse quantum confinement effect in case of sample S2.

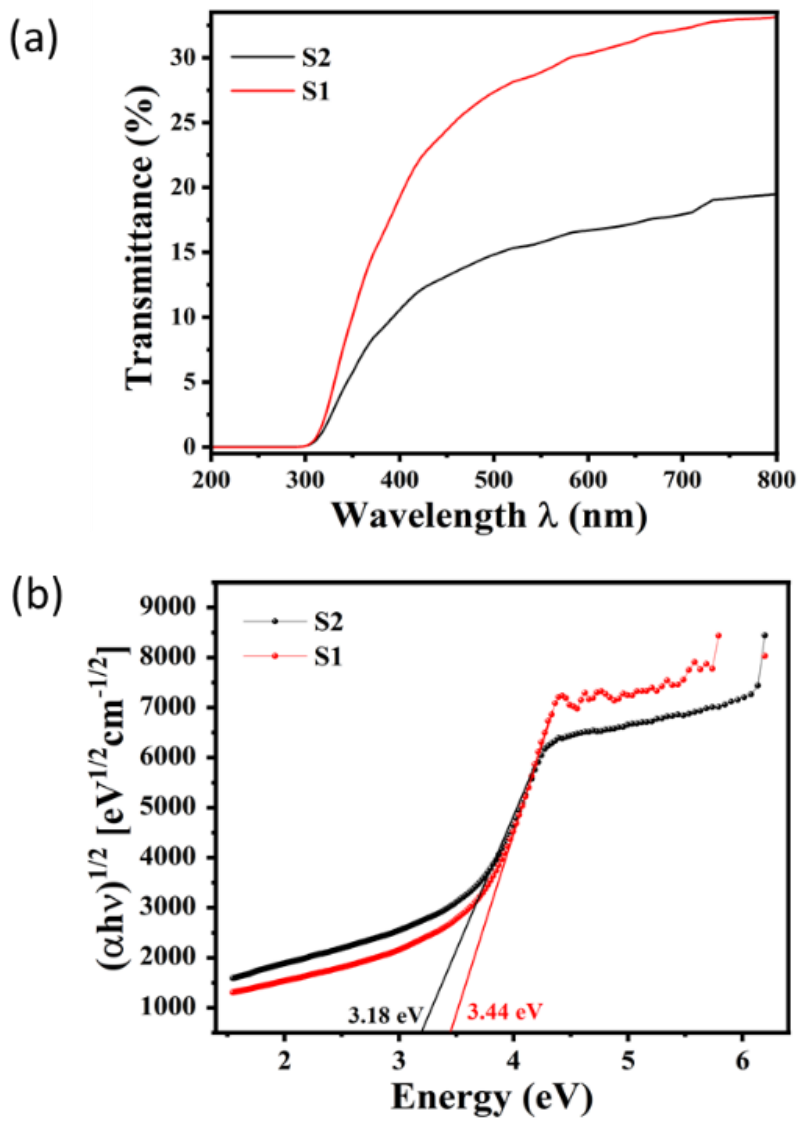

Figure 5. UV-Vis transmittance spectra (a) and Tauc plot (b) for sample S1 and S2.

3.6 TG-DTA Analysis

Figure 6 (a) presents the thermal stability analysis of pure MoS_2 using TG-DTA characteristics. The temperature was varied from ambient to 700° C. TGA plot shows that the sample maintains good thermal stability within this range, with a maximum weight loss of only 2%. Polymer-based samples were not studied under these conditions, as polymers typically degrade at such high temperature (around 700° C). The DTA curve, shown in **Figure 6 (b)**, exhibits a featureless pattern, indicating the absence of any significant endothermic or exothermic reactions, which aligns with the TGA results that show no prominent mass loss. These findings collectively confirm the excellent thermal stability of the MoS_2 samples.

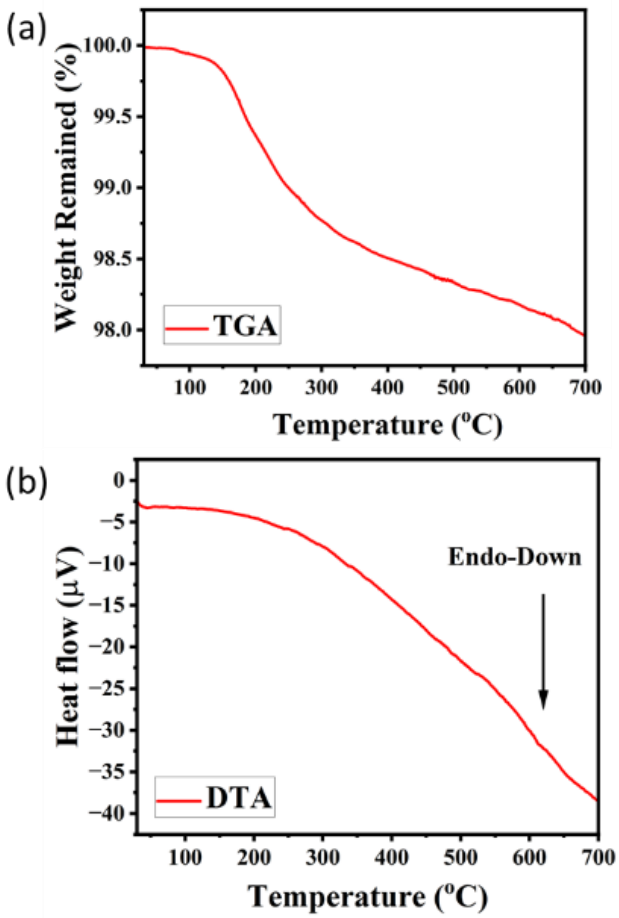

Figure 6. TGA (a) and DTA (b) plot of pure MoS_2.

4. Conclusion

In summary, this study successfully synthesized MoS_2 using a hydrothermal method and integrated it into a PVA matrix to form PVA-MoS_2 composites. The XRD analysis showed enhanced crystallinity in the polymer upon MoS_2 incorporation, suggesting structural improvements. FESEM confirmed the formation of fractal-like MoS_2 clusters, while EDX verified the stoichiometric purity of the composite. UV-Vis spectroscopy and Tauc plot analysis revealed a reduction in the optical band gap from 3.44 eV to 3.18 eV, which is crucial for enhancing the material's optical properties. FTIR confirmed various bonding characteristics, and TG-DTA analysis demonstrated the excellent thermal stability of the samples.

It thus may be concluded that the structural as well as optical properties of polymer may be tuned by changing the dose amount of the reinforcing material MoS_2 which has significant implications for future research, particularly in enhancing the structural, optical, and thermal properties of polymer-based nanocomposites. The change in the optical band gap and increased crystallinity, highlights the potential of PVA-MoS_2 composite for various applications especially in optoelectronics and sensors. Further exploration of these materials could pave the way for the development of high-performance, flexible and stable devices in these fields.

Conflict of Interest

The authors declare that they have no known competing financial interests or personal relationships that could have appeared to influence the work reported in this paper.

Acknowledgments

The authors wish to thank Department of Science and Technology (DST, Gov't of India) for the financial support during the execution of the work **(DST/TDT/DDP-52/2021). DB** wants to thank Teerthanker Mahaveer University for providing funding support during execution of this work under seed money scheme **(TMU/R.O/2020=21/Seed Money/028).** AD want to thank Teerthanker Mahaveer University for granting fellowship during the execution of the work.

References

Acerce, M., Voiry, D., & Chhowalla, M. (2015). Metallic 1T phase MoS2 nanosheets as supercapacitor electrode materials. *Nature Nanotechnology*, *10*(4), 313-318.

Anand, K., Kaur, R., Arora, A., & Tripathi, S.K. (2023). Tuning of linear and non-linear optical properties of MoS2/PVA nanocomposites via ultrasonication. *Optical Materials*, *137*, 113523.

Banerjee, D., Jha, A., & Chattopadhyay, K.K. (2012). Synthesis and characterization of water soluble functionalized amorphous carbon nanotube-poly (vinyl alcohol) composite. *Macromolecular Research*, *20*, 1021-1028.

Chang, H., & Wu, H. (2013). Graphene-based nanomaterials: Synthesis, properties, and optical and optoelectronic applications. *Advanced Functional Materials*, *23*(16), 1984-1997.

Chen, W., Tao, X., Xue, P., & Cheng, X. (2005). Enhanced mechanical properties and morphological characterizations of poly (vinyl alcohol)–carbon nanotube composite films. *Applied Surface Science*, *252*(5), 1404-1409.

Cheng, P., Sun, K., & Hu, Y.H. (2016). Memristive behavior and ideal memristor of 1T phase MoS2 nanosheets. *Nano Letters*, *16*(1), 572-576.

Das, S., Gulotty, R., Sumant, A.V., & Roelofs, A. (2014). All two-dimensional, flexible, transparent, and thinnest thin film transistor. *Nano Letters*, *14*(5), 2861-2866.

Gu, W., Yan, Y., Zhang, C., Ding, C., & Xian, Y. (2016). One-step synthesis of water-soluble MoS2 quantum dots via a hydrothermal method as a fluorescent probe for hyaluronidase detection. *ACS Applied Materials & Interfaces*, *8*(18), 11272-11279.

Huang, Y., Guo, J., Kang, Y., Ai, Y., & Li, C.M. (2015). Two dimensional atomically thin MoS 2 nanosheets and their sensing applications. *Nanoscale*, *7*(46), 19358-19376.

Hwang, J., Choi, H.K., Moon, J., Kim, T.Y., Shin, J.W., Joo, C.W., Han, J.H., Cho, D.H., Huh, Choi, S.Y., Lee, J.I., & Yong Chu, H. (2012). Multilayered graphene anode for blue phosphorescent organic light emitting diodes. *Applied Physics Letters*, *100,* 133304.

Kim, H.U., Kim, H., Ahn, C., Kulkarni, A., Jeon, M., Yeom, G.Y., Lee, M.H., & Kim, T. (2015). In situ synthesis of MoS 2 on a polymer based gold electrode platform and its application in electrochemical biosensing. *RSC Advances*, *5*(14), 10134-10138.

Mak, K.F., Lee, C., Hone, J., Shan, J., & Heinz, T.F. (2010). Atomically thin MoS 2: a new direct-gap semiconductor. *Physical Review Letters*, *105*(13), 136805.

Mas-Balleste, R., Gomez-Navarro, C., Gomez-Herrero, J., & Zamora, F. (2011). 2D materials: to graphene and beyond. *Nanoscale*, *3*(1), 20-30.

Naebe, M., Lin, T., Staiger, M.P., Dai, L., & Wang, X. (2008). Electrospun single-walled carbon nanotube/polyvinyl alcohol composite nanofibers: structure–property relationships. *Nanotechnology*, *19*(30), 305702.

Pawbake, A.S., Waykar, R.G., Late, D.J., & Jadkar, S.R. (2016). Highly transparent wafer-scale synthesis of crystalline WS2 nanoparticle thin film for photodetector and humidity-sensing applications. *ACS Applied Materials & Interfaces*, *8*(5), 3359-3365.

Radisavljevic, B., Radenovic, A., Brivio, J., Giacometti, V., & Kis, A. (2011). Single-layer MoS2 transistors. *Nature Nanotechnology*, *6*(3), 147-150.

Ratan, A., Tripathi, A., & Singh, V. (2021). Swift heavy ion beam modified MoS2-PVA nanocomposite free-standing electrodes for polymeric electrolyte based asymmetric supercapacitor. *Vacuum*, *184*, 109992.

Ray, U., Sarkar, S., Sharma, P., Dhariwal, A., Jha, A., Das, N.S., Kumar, S., Banerjee, D., & Chattopadhyay, K.K. (2024). Silica-amorphous carbon nanotube hybrid induced removal of rhodamine B from water. *Silicon*, *16*(1), 415-424.

Shinde, S.M., Kalita, G., & Tanemura, M. (2014). Fabrication of poly (methyl methacrylate)-MoS2/graphene heterostructure for memory device application. *Journal of Applied Physics*, *116*(21), 214306.

Tsai, M.L., Su, S.H., Chang, J.K., Tsai, D.S., Chen, C.H., Wu, C.I., Li, L.J., Chen, L.J., & He, J.H. (2014). Monolayer MoS2 heterojunction solar cells. *ACS Nano*, *8*(8), 8317-8322.

Wang, X., Feng, H., Wu, Y., & Jiao, L. (2013). Controlled synthesis of highly crystalline MoS2 flakes by chemical vapor deposition. *Journal of the American Chemical Society*, *135*(14), 5304-5307.

Wei, R., Zhang, H., Tian, X., Qiao, T., Hu, Z., Chen, Z., He, X., Yu, Y., & Qiu, J. (2016). MoS 2 nanoflowers as high performance saturable absorbers for an all-fiber passively Q-switched erbium-doped fiber laser. *Nanoscale*, *8*(14), 7704-7710.

Xiao, J., Wang, X., Yang, X.Q., Xun, S., Liu, G., Koech, P.K., Liu, J., & Lemmon, J.P. (2011). Electrochemically induced high capacity displacement reaction of PEO/MoS2/graphene nanocomposites with lithium. *Advanced Functional Materials*, *21*(15), 2840-2846.

Yin, Z., Li, H., Li, H., Jiang, L., Shi, Y., Lu, G., Zhang, Q., Chen, X., & Zhang, H. (2012). Single-layer MoS2 phototransistors. *ACS Nano*, *6*(1), 74-80.

Zhou, K.G., Mao, N.N., Wang, H.X., Peng, Y., & Zhang, H.L. (2011). A mixed-solvent strategy for efficient exfoliation of inorganic graphene analogues. *Angewandte Chemie International Edition*, *46*(50), 10839-10842.

Publisher's Note- Ram Arti Publishers remains neutral regarding jurisdictional claims in published maps and institutional affiliations.